Narrow electroluminescence in bromide ligand-capped cadmium chalcogenide nanoplatelets

Yi Tian Thung,[1,2] Zitong Zhang,[1] Fei Yan,[2] Hilmi Volkan Demir,[1,2,3,4,a] (iD) and Handong Sun[1,a] (iD)

AFFILIATIONS

[1]Division of Physics and Applied Physics, School of Physical and Mathematical Sciences, Nanyang Technological University, 21 Nanyang Link, Singapore 637371, Singapore

[2]LUMINOUS! Centre of Excellence for Semiconductor Lighting and Displays, The Photonics Institute, School of Electrical and Electronic Engineering, Nanyang Technological University, Singapore 639798, Singapore

[3]School of Materials Science and Engineering, Nanyang Technological University, Singapore 639798, Singapore

[4]Department of Electrical and Electronics Engineering, Department of Physics, UNAM—Institute of Materials Science and Nanotechnology, Bilkent University, Ankara 06800, Turkey

[a]Authors to whom correspondence should be addressed: hvdemir@ntu.edu.sg and hdsun@ntu.edu.sg

ABSTRACT

Colloidal zinc blende II–VI semiconductor nanoplatelets (NPLs) demonstrate as a promising class of materials for optoelectronic devices due to their unique excitonic characteristics, narrow emission linewidth, and quantum well-structure. Adopting heterostructures for these nanocrystals allows tuning of their optical features and enhances their photostability, photoluminescence (PL), quantum yield (QY), and color purity for further device integration. Exchanging of carboxylate capping ligands on top and bottom [001] facets of CdSe NPLs with halide ligands is an alternative to achieve the aims of spectral tunability and improve surface passivation, but to date there have been no reports on integrating the advantages of halide ligand exchanged CdSe NPLs for device fabrication. In this work, we demonstrate green electroluminescence (EL) of bromide ligand-capped CdSe NPLs as active emitters in an electrically driven light emitting diode (LED) with a low turn-on voltage of 3.0 V. We observed EL emission at 533.1 nm with a narrow linewidth of 19.4 nm, a maximum luminance of 1276 cd/m^2, and the highest external quantum efficiency (EQE) of 0.803%. These results highlight the ability of halide ligand exchange in tuning the EL properties of CdSe NPL-LEDs and potential of bromide ligand-capped CdSe NPLs in contributing to the green emission region of NPL-LEDs, demonstrating its potential for future device integration and contribution to a high color rendering index of future NPL displays.

Colloidal cadmium chalcogenide nanoplatelets (NPLs) emerged as a promising class of quasi-2D semiconductor nanocrystals for optoelectronic and photonic applications over the past decade. The quantum confinement along their vertical direction assures that these 2D NPLs possess unique thickness-dependent optical properties of the narrow emission linewidth due to suppressed inhomogeneous broadening, reduced Auger recombination, giant oscillator strength, and large absorption coefficient.[1–9] Their distinctive properties bestow potential for NPLs to be integrated in a wide range of optoelectronic applications such as solar energy harvesting,[10,11] lasers,[12–15] and light emitting diodes (LEDs).[16–21] The attributes of high color purity, narrow full-width at half-maximum (FWHM), facile bottom-up solution-processed synthesis, and ease of compatibility with flexible electronics[18,20,21] made NPLs a highly promising candidate for next-generation lighting and display applications. To tap on such potential, extensive efforts have been dedicated to explore the tunability of excitonic features and improve NPLs' surface passivation through implementing heterostructures through core–shell,[16,19–23] core–crown,[17,21] or core-crown-shell structures,[24] doping,[25,26] and alloying,[27–30] which helps to increase their photoluminescence (PL) quantum yield (QY) and photostability for further device integration.

In employing heterostructured NPLs, Liu *et al.*[20] reported highly saturated red-emitting NPL-LEDs employing core/shell CdSe/Cd$_{0.25}$Zn$_{0.75}$S NPLs synthesized via the hot-injection shell growth method giving a record high external quantum efficiency (EQE) of 19.2%. Zhang *et al.*[17] demonstrated green-emitting core/crown CdSe/CdS NPL-LEDs with an

EQE of 5% and high spectral purity. Despite good performance, these heterostructure NPL-LEDs lack flexibility in spectral tunability as core/shell NPLs emit luminescence in the red region of the visible spectra, while core/crown NPLs see tunable emission occurring at discrete wavelengths as a function of the core's thickness. For next-generation lighting applications of NPLs, particularly when aiming toward the high color rendering index for white light emission, precise spectral tunability is desirable. Altintas et al.[29] showed how the spectral tunability issue can be addressed through a combination of core/shell heterostructure NPLs with alloyed core and/or shell components, giving NPLs with varying peak emission from 554 to 650 nm to enable NPL-LEDs with controlled electroluminescence (EL) emission from green to deep-red regions. Together with existing works demonstrating EL from NPLs at 515[31] and 520 nm,[27] further efforts are necessary to demonstrate the EL in the spectral range of 530 nm to improve NPL EL emission in the green region if the high color rendering index is aimed.

Recently, it has been shown that exchanging of carboxylate capping ligands on top and bottom [001] facets of core CdSe NPLs with halide ligands can achieve passivation of surface traps along with tuning of the optical features. Dufour et al.[32] demonstrated, in a 2019 work, an increase in the PL QY to 70% ± 10% from the contemporary 20% from zinc blende four monolayer (ML) CdSe NPLs after exchanging acetate and oleate ligands with bromide and olelyamine ligands. A red shift of emission from 514 to 527 nm and associated absorption profiles observed after ligand exchange, attributed increasing NPL thickness from lattice strain induced to contract NPLs laterally and expand perpendicularly, also indicates the ability of thickness tunability and controlling of optical features through ligand tuning. Moreover, the short length of halide ligands made them desirable in applications involving charge transport such as field effect transistors[33] and solar cells.[34] The work of Dufour et al.[32] offered an alternative for spectral tunability through changing the thicknesses of core NPLs and the possibility for EL emission in the 530 nm region. However, to date there has been no effort in implementing halide ligand exchange NPLs in LEDs; Dufour et al. previously implemented them in a conventional LED structure proposed by Dai et al.[35] but did not observe significant EL output.

In this Letter, we present the integration of bromide ligand exchange NPLs or CdSe–Br NPLs as an emitting layer in a functionable NPL-LED. The improvement in device performance over previously reported works in the literature is attributed to the selection of a device architecture that allows for hole and electron transport materials, which are better compatible with CdSe-Br NPLs in terms of the energy level alignment and charge transport properties to improve the EL efficiency. The as-fabricated NPL-LEDs demonstrate an EL spectrum peaking of 533.1 nm with a FWHM of 19.4 nm with the Commission Internationale de L'Eclairage (CIE) coordinates of (0.221, 0.722) and a low turn-on voltage of 3.0 V. The findings in our work highlight the potential of halide ligand exchange NPLs in future lighting and display applications in offering spectral tunability for EL output from NPLs and filling a missing gap in EL emission from NPLs in the pursuit of the high color rendering index in white light generation.

Synthesis of core-only four ML zinc blende CdSe NPLs follows the procedures in the literature[36–38] with slight modifications. Thereafter, bromide ligand exchange was carried out on the core-only four ML CdSe NPLs following our previously reported work.[38] The details regarding NPL synthesis and associated characterization are listed in the Methods section of Notes 1 in the supplementary material. Spectra of optical absorption and PL as well as the values of PL QY before and after the bromide ligand exchange process are depicted in Fig. 1(a). A red shift of optical features along with an increase in the solution PL QY is observed after bromide ligand exchange, which is consistent with the results reported in the literature.[32,38] The maximum PL emission redshifts from 515 to 531 nm, and the FWHM increases from 9.68 to 12.73 nm; heavy-hole and light-hole transitions change from 511 and 479 nm to 526 and 493 nm after ligand exchange, respectively. Such a red shift of optical properties is proposed by Dufour et al.[32] to be the result of bromide ligands reducing stresses induced by the previous carboxylate ligands, causing unfolding of NPLs that reduces their surface areas and increases their thicknesses simultaneously, which is in line with the understanding of quantum confinement effects of 2D quantum well structures.[1] In our previous work,[38] the surface depletion model that is prominent in NPLs due to their small vertical thickness and large surface-to-volume
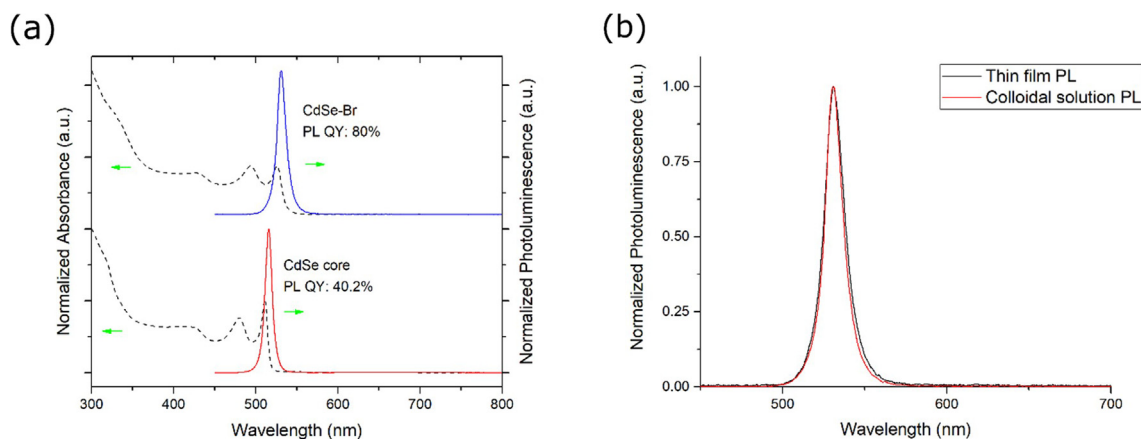

FIG. 1. (a) Normalized absorbance and photoluminescence spectra of 4 ML bromide ligand-capped CdSe NPLs and core-only CdSe NPLs at room temperature. Corresponding PL QYs are indicated in the graph. (b) Normalized photoluminescence spectra of four ML bromide ligand-capped CdSe NPLs in the thin film and the solution form.

ratio is proposed to account for the red shift as well as an increase in the PL QY.

While the bromide ligand-capped NPLs obtain a high PL QY in the solution form, a maximum of 19% is observed for the thin film. The contrast between the values is likely a result of NPLs stacking on the thin film, resulting in reabsorption effects and nonradiative energy transfer attributed to their small Stokes shift. From Fig. 1(b), a comparison between the normalized photoluminescence of the bromide ligand-capped NPLs in a solution and a thin film shows little red shift and changes in the FWHM. This indicates the feasibility of integrating the bromide ligand-capped NPLs as a thin film onto the substrate for further device applications. The transmission electron microscopy (TEM) images of NPLs before and after the bromide ligand exchange process are displayed in Figs. 2(a) and 2(b), respectively. From the images, the 2D-shape of NPLs is preserved after the ligand exchange process, and a significant reduction of NPL stacking with improved monodispersity is observed. From Fig. 2(a), the original CdSe NPLs capped by acetate and oleaste ligands show prominent stacking of their [001] facets, which was significantly reduced when the NPLs are instead capped by bromide and oleylamine ligands. The reduction in stacking and improved monodispersity of NPLs after bromide ligand exchange can significantly reduce undesirable nonradiative energy

transfer, contributing to improved PL QY in addition to improving surface passivation and redshifting optical properties. Such observations, hence, indicate the promises of the bromide ligand-capped NPLs to be employed in device aspects in the form of a thin film on a substrate.

In an attempt to incorporate four ML CdSe–Br NPLs in a LED with a conventional device architecture, Dufour et al.[32] attributed the low EL efficiency achieved to the unsuitability of the device structure; their device structure and materials used for hole and electron transport were optimized for core–shell NPLs instead of bromide-capped NPLs. Hence, our work identifies the importance of realizing EL from CdSe–Br NPLs in a suitable LED structure that allows for flexibility in the choice of materials of neighboring layers that are compatible with a CdSe–Br NPLs' emitting layer (EML). The inverted LED device architecture is identified as a suitable alternative from various perspectives of considerations. The deep-lying valence band of the NPLs notices the need for hole transport layer (HTL) materials with comparable deep lying high-occupied-molecular-orbital (HOMO) levels to ensure proper hole injection into the NPL EML in the device. Compared to the conventional LED structure adopted by Dufour et al.,[31] the inverted structure adopted in this work allows for a wider selection of organic small molecule materials with high-hole mobility as the hole transport layer (HTL) for better energy level alignment with the CdSe–Br NPLs. This is due to the fact that the HTL is incorporated via thermal evaporation in the inverted structure compared to solution-processed methods in the conventional structure; the latter limits the choice of HTL materials to those soluble in a suitable solvent. For evaluation of EL properties of CdSe–Br NPL-based devices, the as-synthesized four ML CdSe–Br NPLs were integrated in an inverted LED with a device architecture of indium tin oxide (ITO)/zinc oxide (ZnO)/NPLs/tris(4-carbazoyl-9-ylphenyl)amine (TCTA)/molybdenum oxide (MoO_3)/aluminium (Al) as shown in Fig. 3(a). Subsequent studies were then conducted on the LEDs with an area of $1 \times 1 \, mm^2$.
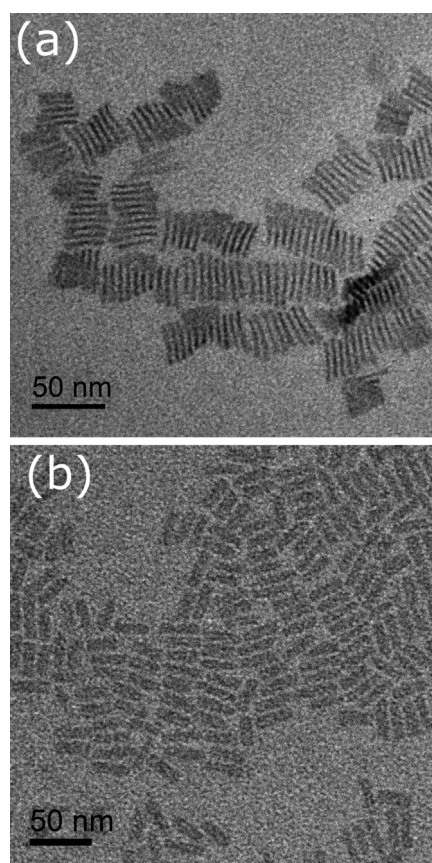

FIG. 2. TEM images of (a) four ML CdSe core-only NPLs and (b) bromide ligand-capped CdSe NPLs after going through bromide treatment.
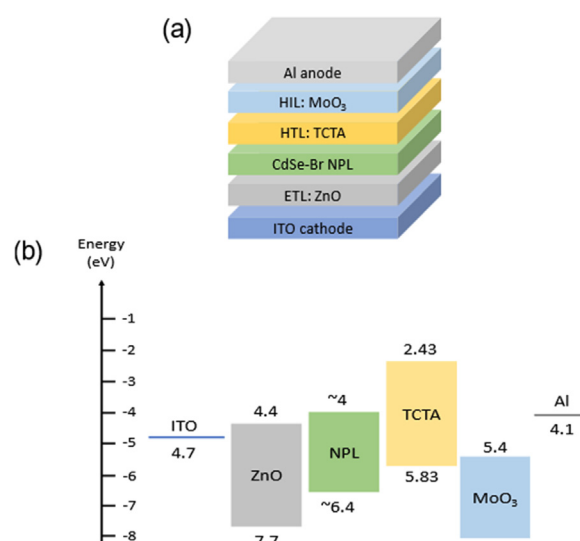

FIG. 3. (a) Schematic representation of the NPL-LED architecture adopted for this work and (b) the proposed flatband energy diagram of the NPL-LEDs. The values are taken from Refs. 20, 35, and 39–41.

The device fabrication specifics are described in the Methods section of Notes 1 in the supplementary material. For this inverted LED architecture, the ITO functions as the cathode, the ZnO nanocrystal film as an electron injecting layer, CdSe–Br NPLs as the emitting layer, TCTA and MoO_3 as the hole transport and injection layers, respectively, and Al as the anode.

Taking reference with the conduction and valence band edge values of CdSe NPLs to be 4.3 and 6.0 eV, respectively,[20,35,39] the band edge values of CdSe–Br are expected not to deviate significantly from that of the CdSe NPLs. The electron transport, hole transport, and hole injection layers must be chosen from materials that are well aligned with the energy levels of the NPLs. From Fig. 3(b), ZnO with a conduction band value[35] of ~4.4 eV is well aligned with the conduction band of the NPLs, and the position of its valence band[35] at ~7.7 eV allows it to function as a hole blocking layer. Their high electron mobility at 1.8×10^{-3} cm^2 V^{-1} s^{-1} also ensures efficient electron injection into the NPLs.[35] In the selection of hole transport materials, TCTA is identified as a suitable candidate due to its high-lying lowest-unoccupied-molecular-orbital (LUMO) and low-lying HOMO; the HOMOs of TCTA at 5.83 eV[40,41] are well aligned with the valence band of NPLs for hole transport, while its high-lying LUMO at

2.43 eV[40,41] theoretically allows it to function as an electron blocking layer, working in tandem with the ZnO electron transport layer to confine radiative recombination within the NPL emitting layer. The hole mobility of TCTA is 3×10^{-4} cm^2 V^{-1} s^{-1},[40] making it an efficient hole transport material.

Figure 4(a) shows the current density–luminance–voltage characteristics of the as-fabricated NPL-LED following the inverted structure in Fig. 3(a). The turn-on voltage, which is defined as the driving voltage when the brightness of the device reaches 1 cd m^{-2}, is at a low value of 3.0 V. A maximum brightness of 1276 cd/m^2 is achieved at a driving voltage of 7.6 V with the maximum EQE achieved for this device at 0.803%. Figure 4(b) shows the electroluminescence spectra from the fabricated LED at various operating voltages. The device produces pronounced EL emission peaks centered around 534 nm with the peak at a driving voltage of 7 V having a FWHM of 21.1 nm. At higher driving voltages, broadening of the EL peak is attributed to longitudinal optical phonon coupling, where larger exciton polarization is expected with stronger electric fields.[42,43] This fabricated LED pioneers NPL-LED emission in the ~530 nm region and also for NPL-LEDs using core-only CdSe NPLs as the EML producing narrow EL. From a comparison between the normalized PL and EL emissions from the
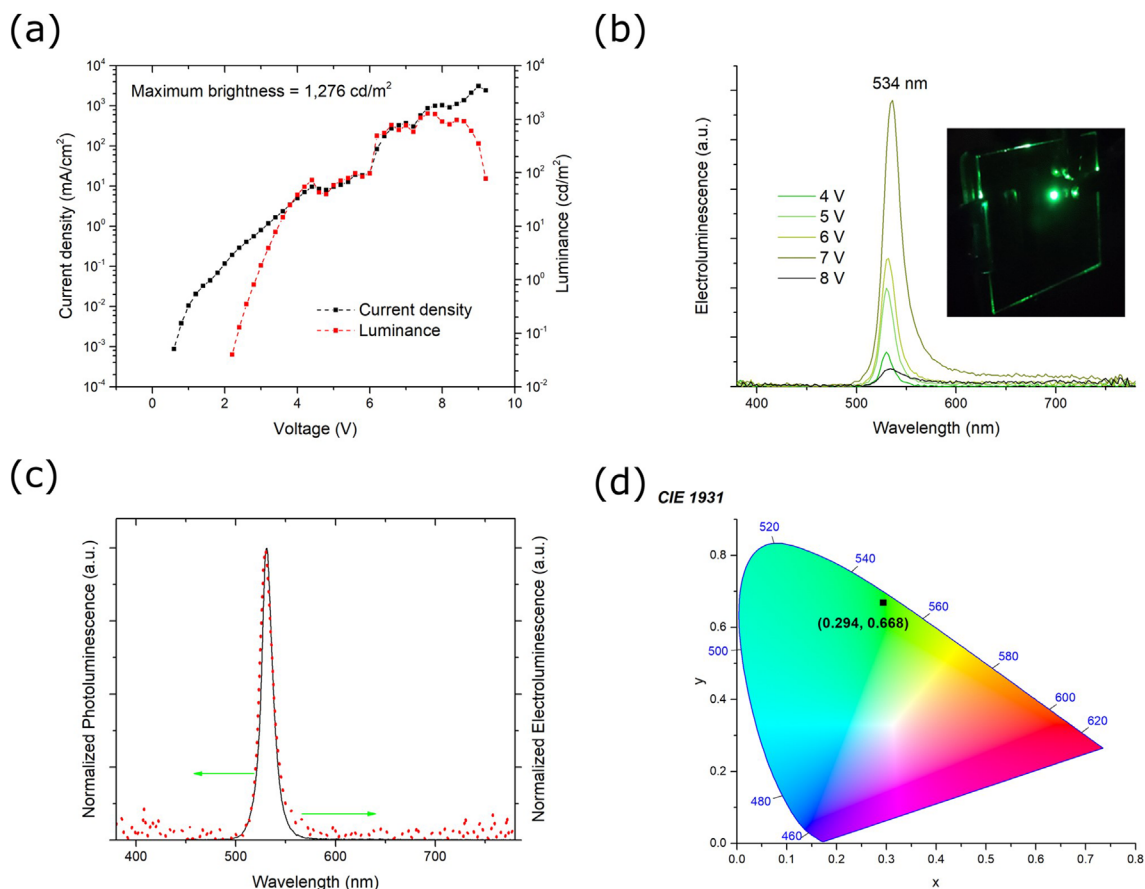

FIG. 4. Device characterization of the NPL-LEDs. (a) Current density-voltage-luminance characteristics of NPL-LED fabricated. (b) Electroluminescence spectra of the NPL-LED with the inset showing an image of the fabricated LED. (c) Comparison of normalized photoluminescence from four ML bromide ligand-capped CdSe NPLs and electroluminescence from the fabricated NPL-LED. (d) Position of the coordinates (0.294, 0.668) in the CIE 1931 diagram.

CdSe-Br NPL solution and the as-fabricated device, respectively, as shown in Fig. 4(c), we observe only a slight increase in the FWHM of the peak and a minor red shift of 3 nm. This affirms that the EL emitted from the as-fabricated LED is solely from the NPL EML, and there is no parasitic emission from neighboring layers from our measurements conducted.

Compared to the previous attempt to incorporate the bromide ligand-capped CdSe NPLs into LEDs,[32] the improved EL performance is attributed to the greater suitability of the inverted LED structure, allowing TCTA to be employed as the HTL, which was previously impossible when adopting the conventional structure. The confinement of EL emission to be from the NPL EML solely is attributed to how the ZnO ETL and TCTA HTL adopted prevent overflowing of holes and electrons, respectively, ensuring all radiative recombination to occur solely in the NPL EML. The measurements taken also affirm the theoretical speculation on how the TCTA HTL complements the ZnO ETL for proper charge injection toward the NPL EML layer from the perspective of their charge mobilities. The fabricated LED, hence, emits green EL as shown in the inset of Fig. 4(c); from Fig. 4(d), the CIE 1931 coordinates of the emission are at (0.294, 0.688). The integration of the bromide ligand-capped NPLs demonstrated how the halide ligand exchange process can be employed for precise spectral tunability of NPL-LED's EL emission and, thus, contains potential in improving the color rendering index of NPLs for lighting applications in white emission.

Despite the promising performance of the as-fabricated LED, the device shows reduced luminance after 8 V with device failure occurring rapidly as seen in Fig. 4(a); the device also has less stellar performance when compared to heterostructure NPL-LEDs. The instability of the device and subsequent breakdown at higher driving voltages can be understood from a material aspect. Compared to the core/shell and core/crown NPLs,[17,18,20,21] the bromide ligand-capped NPLs adopted in this work lack a well-defined heterostructure. Their heterostructure counterparts, such as core–shell or core–crown structure, have shown greater stability and optical performance, attributed to the heterojunction confining the excitonic wave function within the core component and reducing opportunity to visit surface defects. As a result, heterostructured NPLs demonstrate higher PL QY and stability compared to core-only NPLs. While the exchange of acetate and oleate ligands to bromide and oleylamine ligands helps it to reduce the NPL stacking and improve the PL QY, it does not provide a heterostructure. Furthermore, it has been stated by Dufour *et al.* and in our previous work[32,38] that delocalization of the excitonic wave function on the bromide layer takes place in the bromide ligand-capped NPLs. As a result, the exciton wave function in bromide ligand-capped NPLs is less confined within the core and realizes greater opportunity to visit surface defects, greatly boosting the chance of nonradiative recombination at surface traps, which not only reduce device efficiency but also contribute as a source of Joule heating, which is a problem common in NPL-LEDs.[44]

These issues manifest as limitations on device performance evident in Fig. 4(b). The jittering of both the current density and luminance is beyond 4 V point toward slight operational instability with increasing driving voltage. This is speculated to be a result of the excitonic wave function delocalizing toward the bromide layer on the NPL surface, causing partial charge carrier drift through the NPL active layer and resulting in a small extent of recombination at the HTL, an issue observed in NPL-LEDs by employing NPLs without a

heterostructure.[31] With some recombination occurring at the HTL, the as-fabricated NPL-LED shows EL from the TCTA layer, accounting for the trailing of the EL spectra at longer wavelengths as seen in Fig. 4(b), and the asymmetry at long wavelengths when compared to the Pl spectra in Fig. 4(c). From Fig. 4(b), luminance from the fabricated LED drops rapidly beyond 8 V, where simultaneously current density increases beyond 1000 mA/cm^2; this significant fall in device efficiency can then be partially attributed to Joule heating, burning through the layers on the as-fabricated device, which is observed experimentally and results in device failure after 9.2 V. While further studies are essential to resolve the present inadequacies of NPL-LEDs employing bromide ligand exchange NPLs, the experimental data have shown utmost potential for the halide ligand exchange process in tuning the EL emission from NPLs and the potential for bromide ligand-capped CdSe NPLs for further device applications.

In summary, we investigated the integration of bromide ligand-capped four ML CdSe NPLs as an emitting layer into an inverted architecture hybrid LED by employing inorganic ETL and organic HTLs and demonstrated pronounced EL. We synthesized bromide ligand-capped CdSe NPLs with a PL emission of 531 nm, a FWHM of 12.73 nm, and a solution PL QY of 80%, which were then used in fabrication of an inverted LED, with the device having a low turn-on voltage of 3.0 V, and demonstrated EL emission at 534 nm with a FWHM of 21.1 nm, a maximum brightness of 1276 cd/m^2, an EQE of 0.803%, and CIE 1931 coordinates of (0.294, 0.668). The EL emission achieved in this work also contributed to spectral tunability of NPL-LEDs, filling a gap in pursuit of the high color rendering index for next-generation NPL lighting applications. We identified the factors limiting device performance in this work, which retrospectively helps us to understand the need for further actions to improve compatibility of bromide ligand-capped CdSe NPLs in NPL-LEDs. Our work highlights how the halide ligand exchange process can contribute toward EL emission tuning and the potential of the halide ligand-capped CdSe NPLs in future optoelectronic applications.

See the supplementary material for specifications on chemicals and experimental methods employed.

AUTHOR DECLARATIONS
Conflict of Interest

The authors have no conflicts to disclose.

Author Contributions

Y.T.T. and Z.Z. contributed equally to this work.

DATA AVAILABILITY

The data that support the findings of this study are available from the corresponding authors upon reasonable request.

REFERENCES

[1] S. Ithurria, M. D. Tessier, B. Mahler, R. P. Lobo, B. Dubertret, and A. L. Efros, Nat. Mater. **10**, 936–941 (2011).

[2] M. D. Tessier, C. Javaux, I. Maksimovic, V. Loriette, and B. Dubertret, ACS Nano **6**, 6751–6758 (2012).

[3] C. She, I. Fedin, D. S. Dolzhnikov, A. Demortière, R. D. Schaller, M. Pelton, and D. V. Talapin, Nano Lett. **14**, 2772–2777 (2014).

[4] K. Wu, Q. Li, Y. Jia, J. R. McBride, Z.-X. Xie, and T. Lian, ACS Nano **9**, 961−968 (2015).

[5] A. Naeem, F. Masia, S. Christodoulou, I. Moreels, P. Borri, and W. Langbein, Phys Rev B. **91**, 121302 (2015).

[6] A. Yeltik, S. Delikanli, M. Olutas, Y. Kelestemur, B. Guzelturk, and H. V. Demir, J. Phys. Chem. C **119**, 26768–26775 (2015).

[7] R. Vaxenburg, A. Rodina, E. Lifshitz, and A. Efros, Nano Lett. **16**, 2503–2511 (2016).

[8] C. Bouet, M. D. Tessier, S. Ithurria, B. Mahler, B. Nadal, and B. Dubertret, Chem. Mater. **25**, 1262–1271 (2013).

[9] S. J. Zelewski, K. C. Nawrot, A. Zak, M. Gladysiewicz, M. Nyk, and R. Kudrawiec, J. Phys. Chem. Lett. **10**, 3459–3464 (2019).

[10] S. Luo, M. Kazes, H. Lin, and D. Oron, J. Phys. Chem. C **121**, 11136−11143 (2017).

[11] M. Sharma, K. Gungor, A. Yeltik, M. Olutas, B. Guzelturk, Y. Kelestemur, T. Erdem, S. Delikanli, J. R. McBride, and H. V. Demir, Adv. Mater. **29**, 1700821 (2017).

[12] B. Guzelturk, Y. Kelestemur, M. Olutas, S. Delikanli, and H. V. Demir, ACS Nano **8**, 6599–6605 (2014).

[13] J. Q. Grim, S. Christodoulou, F. D. Stasio, R. Krahne, R. Cingolani, L. Manna, and I. Moreels, Nat. Nanotechnol. **9**, 891–895 (2014).

[14] M. Li, M. Zhi, H. Zhu, W.-Y. Wu, Q.-H. Xu, M. H. Jhon, and Y. Chan, Nat. Commun. **6**, 8513 (2015).

[15] Z. Yang, M. Pelton, L. Fedin, D. V. Talapin, and E. Waks, Nat. Commun. **8**, 143 (2017).

[16] Z. Chen, B. Nadal, B. Mahler, H. Aubin, and B. Dubertret, Adv. Funct. Mater. **24**, 295–302 (2014).

[17] F. Zhang, S. Wang, L. Wang, H. Shen, W. Cao, C. Yang, H. Wang, L. Yu, Z. Du, J. Xue, and L. S. Li, Nanoscale **8**, 12182–12188 (2016).

[18] B. Liu, S. Delikanli, Y. Gao, D. Dede, K. Gungor, and H. V. Demir, Nano Energy **47**, 115–122 (2018).

[19] Y. Kelestemur, Y. Shynkareno, M. Anni, S. Yakunin, M. L. De Giorgi, and M. V. Kovalenko, ACS Nano **13**, 13899–13909 (2019).

[20] B. Liu, Y. Altintas, L. Wang, S. Shendre, M. Sharma, H. D. Sun, E. Mutlugun, and H. V. Demir, Adv. Mater. **32**, 1905824 (2020).

[21] Z. Wen, P. Liu, J. Ma, S. Jia, X. Xiao, S. Ding, H. Tang, H. Yang, C. Zhang, X. Qu, B. Xu, K. Wang, K. L. Teo, and X. W. Sun, Adv. Electron. Mater. **7**, 2000965 (2021).

[22] Y. Altintas, K. Gungor, Y. Gao, M. Sak, U. Quiliyeva, G. Bappi, E. Mutlugun, E. H. Sargent, and H. V. Demir, ACS Nano **13**, 10662–10670 (2019).

[23] Y. Altintas, U. Quliyeva, K. Gungor, O. Erdem, Y. Kelestemur, E. Mutlugun, M. V. Kovalenko, and H. V. Demir, Small **15**, 1804854 (2019).

[24] S. Shendre, S. Delikanli, M. Li, D. Dede, Z. Pan, S. T. Ha, Y. H. Fu, P. L. Hernandez Martinez, J. Yu, O. Erdem, A. I. Kuznetsov, C. Dang, T. C. Sum, and H. V. Demir, Nanoscale **11**, 301–310 (2019).

[25] A. Sharma, M. Sharma, K. Gungor, M. Olutas, D. Dede, and H. V. Demir, Adv. Opt. Mater. **7**, 1900831 (2019).

[26] B. Liu, M. Sharma, J. Yu, S. Shendre, C. Hettiarachchi, A. Sharma, A. Yeltik, L. Wang, H. D. Sun, C. Dang, and H. V. Demir, Small **15**, 1901983 (2019).

[27] F. Fan, P. Kanjanaboos, M. Saravanapavanantham, E. Beauregard, G. Ingram, E. Yassitepe, M. M. Adachi, O. Voznyy, A. K. Johnston, G. Walters, G.-H. Kim, Z.-H. Lu, and E. H. Sargent, Nano Lett. **15**, 4611–4615 (2015).

[28] N. N. Schlenskaya, Y. Yao, T. Mano, T. Kuroda, A. V. Garshev, V. F. KOzlovskii, A. M. Gaskov, R. B. Vasiliev, and K. Sakoda, Chem. Mater. **29**, 579–586 (2017).

[29] Y. Altintas, B. Liu, P. L. Hernández-Martínez, N. Gheshlaghi, F. Shabani, M. Sharma, L. Wang, H. D. Sun, E. Mutlugun, and H. V. Demir, Chem. Mater. **32**, 7874−7883 (2020).

[30] M. Izmir, A. Sharma, S. Shendre, E. G. Durmusoglu, V. K. Sharma, F. Shabani, H. D. Baruj, S. Delikanli, M. Sharma, and H. V. Demir, ACS Appl. Nano Mater. **5**, 1367−1376 (2022).

[31] A. G. Vitukhnovsky, V. S. Lebedev, A. S. Selyukov, A. A. Vashchenko, R. B. Vasiliev, and M. S. Sokolikova, Chem. Phys. Lett. **619**, 185–188 (2015).

[32] M. Dufour, J. Qu, C. Greboval, C. Methivier, E. Lhuillier, and S. Ithurria, ACS Nano **13**, 5326–5334 (2019).

[33] Z. M. Norman, N. C. Anderson, and J. S. Owen, ACS Nano **8**, 7513–7521 (2014).

[34] J. Tang, K. W. Kemp, S. Hoogland, K. S. Jeong, H. Liu, L. Levina, M. Furukawa, X. Wang, R. Debnath, D. Cha, K. W. Chou, A. Fischer, A. Amassian, J. B. Asbury, and E. H. Sargent, Nat. Mater. **10**, 765–771 (2011).

[35] X. Dai, Z. Zhang, Y. Jin, Y. Niu, H. Cao, X. Liang, L. Chen, J. Wang, and X. Peng, Nature **515**, 96–99 (2014).

[36] C. She, I. Fedin, D. S. Dolzhnikov, P. D. Dahlberg, G. S. Engel, R. D. Schaller, and D. V. Talapin, ACS Nano **9**, 9475–9485 (2015).

[37] Z. Zhang, Y. T. Thung, X. Chen, L. Wang, W. Fan, L. Ding, and H. D. Sun, J. Phys. Chem. Lett. **12**, 191–198 (2021).

[38] Z. Zhang, Y. T. Thung, L. Wang, X. Chen, L. Ding, W. Fan, and H. D. Sun, J. Phys. Chem. Lett. **12**, 9086–9093 (2021).

[39] T. C. Chiang and F. J. Himpsel, *Landolt-Börnstein—Group III Condensed Matter* (Springer, Berlin, 1989), Vol. 23, p. 95.

[40] P. Kathirgamanathan, M. Kumaraverl, N. Bramananthan, and S. Ravichandran, J. Mater. Chem. C **6**, 11622–11644 (2018).

[41] Z.-Q. Zhang, Y.-P. Liu, Y.-F. Dai, J.-S. Chen, D.-G. M, and H.-M. Zhang, Chin. Phys. Lett. **31**, 046801 (2014).

[42] S. A. Empedocles and M. G. Bawendi, Science **278**, 2114–2117 (1997).

[43] V. Wood, M. J. Panzer, J. M. Caruge, J. E. Halpert, M. G. Bawendi, and V. Bulovic, Nano Lett. **10**, 24–29 (2010).

[44] J. Lim, Y. S. Park, and V. I. Klimov, Nat. Mater. **17**, 42–49 (2018).